3D computational parametric analysis of eccentric atheroma plaque: influence of axial and circumferential residual stresses

M. Cilla · E. Peña · M. A. Martínez

Abstract Plaque rupture plays a role in the majority of acute coronary syndromes. Rupture has usually been associated with stress concentrations, which are mainly affected by the plaque geometry and the tissue properties. The aim of this study is to evaluate the influence of morphology on the risk of plaque rupture, including the main geometrical factors, and to assess the role of circumferential and axial residual stresses by means of a parametric 3D finite element model. For this purpose, a 3D parametric finite element model of the coronary artery with eccentric atheroma plaque was developed. Healthy (adventitia and media in areas without atheroma plaque) and diseased (fibrotic and lipidic) tissues were considered in the model. The geometrical parameters used to define and design the idealized coronary plaque anatomy were the lipid core length, the stenosis ratio, the fibrous cap thickness, and the lipid core ratio. Finally, residual stresses in longitudinal and circumferential directions were incorporated into the model to analyse the influence of the important mechanical factors in the vulnerability of the plaque. Viewing the results, we conclude that residual stresses should be considered in the modelling of this kind of problems since they cause a significant alteration of the vulnerable plaque region limits. The obtained results show that the fibrous cap thickness and the lipid core length, in combination with the lipid core width, appear to be the key morphological parameters that play a determinant role in the maximal principal stress (MPS). However, the stenosis ratio is found to not play a significant role in vulnerability related to the MPS. Plaque rupture should therefore be observed as a consequence, not only of the cap thickness, but as a combination of the stenosis ratio, the fibrous cap thickness and the lipid core dimensions.

Keywords Vulnerable plaque · Coronary disease · Lipid core · Parametric finite element analysis · Hyperelastic material · Residual stress · Parametric analysis

Electronic supplementary material The online version of this article (doi:10.1007/s10237-011-0369-0) contains supplementary material, which is available to authorized users.

M. Cilla · E. Peña · M. A. Martínez (✉)
Aragón Institute of Engineering Research (I3A),
University of Zaragoza, Zaragoza, Spain
e-mail: miguelam@unizar.es

M. Cilla · E. Peña · M. A. Martínez
CIBER de Bioingeniería, Biomateriales y Nanomedicina
(CIBER-BBN), Zaragoza, Spain

1 Introduction

Cardiovascular diseases related to atherosclerosis are nowadays primary causes of mortality in the developed world, and it has been calculated that they will become the first cause of death worldwide in 2020 (Lloyd-Jones et al. 2009). Atherosclerosis is the process in which plaques—consisting of deposits of cholesterol and other lipids, calcium and large inflammatory cells called macrophages—are built up in the walls of the arteries causing narrowing (stenosis of the lumen), hardening of the arteries and loss of their elasticity, which leads to a reduction in the blood flow through the vessels. Nevertheless, the most serious damage occurs when the plaque becomes fragile and ruptures (vulnerable plaque). Plaque rupture causes the formation of blood clots that can block blood flow or break off and travel to another part of the circular system, thus producing heart attacks, strokes, difficulty in walking, and eventually gangrene (Kyriacou et al. 1996; Hanke and Lenz 2001; Thubrikar 2007).

Until now, several methods have been used to evaluate the extent and location of atherosclerotic lesions: invasive methods such as IVUS (intravascular ultrasound) or X-ray

angiography and non-invasive methods, which detect indicators of atherosclerosis such as classical risk factors (Lee et al. 1993; Fayad and Fuster 2001; Kips et al. 2008). Identifying vulnerable patients before plaque rupture occurs would help clinicians to provide early treatment as well as to take preventive measures. Many strategies have been proposed to achieve this goal, though available screening and diagnostic methods seem to be insufficient.

The characteristics of vulnerable plaque have been well defined in several pathological studies (Salunke et al. 2001; Naghavi et al. 2003; Fuster et al. 2005; Virmani et al. 2006; VanEpps and Vorp 2007) amongst others. Plaque rupture is believed to be related to plaque morphology, mechanical forces, vessel remodelling, blood conditions (levels of cholesterol, sugar, etc.), chemical environment and lumen surface conditions (inflammation) (Van der Wal and Becker 1999). Regarding the mechanical forces, some authors (Ohayon et al. 2005; Versluis et al. 2006) consider the peak circumferential stress (PCS) as the most important biomechanical factor in the mechanisms leading to rupture of the atherosclerotic plaque and have often used it as a predictor of atherosclerotic plaque rupture location. Previous works have shown that reduced fibrous cap thickness increases the maximal value of the PCS exponentially and leads the cap stress to exceed the rupture threshold of 300 kPa (Lendon et al. 1991; Cheng et al. 1993; Ohayon et al. 2005) when the cap thickness becomes lower than 65 μm (Virmani et al. 2006; Moreno et al. 2002; Finet et al. 2004; Vengrenyuk et al. 2006).

The fibrous cap thickness has typically been identified as the key predictor of vulnerability and likelihood of rupture, but some clinical and biomechanical studies have shown that this single parameter is not a reliable predictor of plaque stability (Virmani et al. 2000; Krishna Kumar and Balakrishnan 2005), since plaque stability also depends on other intrinsic properties of the plaque, such as the size and the consistency of the soft atheroma core (Finet et al. 2004; Gao and Long 2008), the cap and the core inflammation levels (Arroyo and Lee 1999; Lee 2000) and the arterial remodelling index, which is defined as the external elastic membrane area at plaque divided by the external elastic membrane area at a nearest segment judged to be free of plaque (Smedby 1998; Varnava et al. 2002; Ohayon et al. 2008).

Several parametric studies have been carried out with two-dimensional models (2D) assuming a plane strain hypothesis in order to study the mechanical risk factor for vulnerable plaque (Ohayon et al. 2005; Cheng et al. 1993; Finet et al. 2004; Lee 2000; Krishna Kumar and Balakrishnan 2005; Ohayon et al. 2008). Nevertheless, other studies show that 2D structural analyses tend to overestimate the maximal value of the PCS (Ohayon et al. 2005). In addition, longitudinal residual stress effects and other features such as the anisotropy or the longitudinal length of the plaque cannot be considered in 2D models.

Several studies have shown the importance of including residual stresses (RS) on arterial models to get an accurate calculation of the stress distribution across the arterial wall (Jaroslav et al. 1999; Peterson and Okamoto 2000; Jaroslav et al. 2002; Raghavan et al. 2004; Ohayon et al. 2007; Alastrué et al. 2007). However, the influence of RS on the wall stress distribution in pathological coronaries remains unclear since the relationship between RS and atheroma plaque configuration is very complex. Longitudinal and axial RS present in a vulnerable coronary plaque dramatically influences the spatial stress distribution and could cause new sites of stress concentration. RS could play a major role in the biomechanical stability of vulnerable coronary plaque and in the growth process of the lipid core. This study shows that plaque rupture is to be viewed as a consequence not only of external pressure but rather of a subtle combination of external loading, geometrical configuration, and intraplaque RS.

Even though the performance and importance of 3D models have been demonstrated to identify vulnerable plaques (Ohayon et al. 2005; Chun et al. 2010), to the best of the authors knowledge, no idealized and parametric 3D studies have attempted to analyse the influence of residual stresses on the biomechanical stability of vulnerable coronary plaques. The performed 3D studies related to the atheroma plaque are usually carried out on geometries obtained from IVUS or MRI (Magnetic Resonance Imaging) (Ohayon et al. 2005; Auer et al. 2006; Briley-Saebo et al. 2007) and residual stresses are neglected. For this reason, the goal of this study is to present a 3D parametric study of the geometric risk factors in an idealized coronary vessel to quantify and investigate the biomechanical interaction between the most influential values of the geometry of the vessel in the plaque rupture: (i) the fibrous cap thickness; (ii) the stenosis ratio; (iii) the lipid core width; and (iv) the lipid core length. Furthermore, the influence of residual stresses on the risk of atheroma plaque has been shown by comparing three set of idealized 3D geometries incorporating residual stresses (one set taking account just the longitudinal RS and other with the longitudinal and the circumferential RS included) and without them.

2 Materials and methods

2.1 Idealized geometry

An idealized geometry corresponding to a coronary vessel with atheroma plaque was modelled. The plaques were characterized by a large lipid pool with a thin fibrous cap (Davies 1996; Ohayon et al. 2001; Finet et al. 2004). Atherosclerotic vessel morphology and average dimensions were obtained from Versluis et al. (2006) and Bluestein et al. (2008). A vessel length of 20 mm, an external radius of 2 mm, and a vessel wall thickness of 0.5 mm were considered to create the basic geometry.

A 3D parametric study of the influence of the geometric factors was performed to check the vulnerability of the atherosclerotic plaque. For this purpose, a 3D finite element model was developed in the commercial finite element code ABAQUS 6.9, taking into account both the composition and the dimensions of the different layers of the tissue (media and adventitia), the fibrous plaque and the lipid core.

The arterial wall was assumed as a hollow cylinder, and the lumen was consider circular. The atherosclerotic plaque, which is located inside the vessel, was assumed to be symmetric with respect to the central cross-section. Finally, the lipid core was approximated as a blunt volume (see Fig. 1). In areas with atheroma plaque, the whole media layer was considered as fibrotic, whereas only the adventitia was considered to be a healthy layer.

The parametric model consists of a series of idealized plaque morphology models, mimicking different stages and variations of the atherosclerotic lesion growth. Following previous works (Cheng et al. 1993; Williamson et al. 2003; Finet et al. 2004; Ohayon et al. 2008), the most influential geometric parameters considered were the fibrous cap thickness (fc), the stenosis ratio (sr)—which is obtained by dividing the lumen radius by the lumen radius of a normal artery ($R = 1.5\,\text{mm}$), $sr(\%) = \frac{r(\text{mm})}{R(\text{mm})}100$—the lipid core length ($l$) and the lipid core width (w). The lipid core width (w) was defined as the ratio between the percentage of the atheroma plaque width (w_1) and the distance from the inner point of the lipid core to the outer point of the fibrotic plaque (w_2), $w(\%) = \frac{w_1(\text{mm})}{w_2(\text{mm})}100$. The central section of the 3D model is shown in Fig. 1b, where the lipid core length was measured along the longitudinal direction (Fig. 1a).

Five values for each parameter were considered and combined which makes a total of 625 idealized eccentric vessel models with atherosclerotic lesions. Realistic morphological data were investigated by varying the lipid core length ($1 \le l \le 8$, in mm), the stenosis ratio ($46.7 \le sr \le 66.7$, in %), the fibrous cap thickness ($0.025 \le fc \le 0.25$, in mm) and the lipid core width ($30 \le w \le 90$, in %) (Fujii et al. 2005). The values of the geometrical parameters used to define the idealized coronary plaque models are shown in Table 1.

Table 1 Geometrical parameters used to generate the parametric 3D models

Level	l (mm)	sr (%)	fc (mm)	w (%)
1	1	46.7	0.025	30
2	2	53.3	0.05	45
3	4	56.7	0.1	60
4	6	60	0.15	75
5	8	66.7	0.25	90

In order to demonstrate the important influence of the longitudinal and circumferential residual stresses in the vulnerability of the plaque, the 625 models were simulated under three different hypothesis: (i) without RS, (ii) just considering axial RS and (iii) taking account both circumferential and axial RS. In total, 1875 analyses have been performed.

A fine mesh was created in the various regions of the model, and the fibrous cap region was meshed with an adaptive mesh. Previous sensitivity analyses were performed on the mesh to choose the definitive one. Due to the symmetry of the problem, only a quarter of the model with approximately 150.000 linear and hybrid tetrahedral elements and 30.000 nodes was considered.

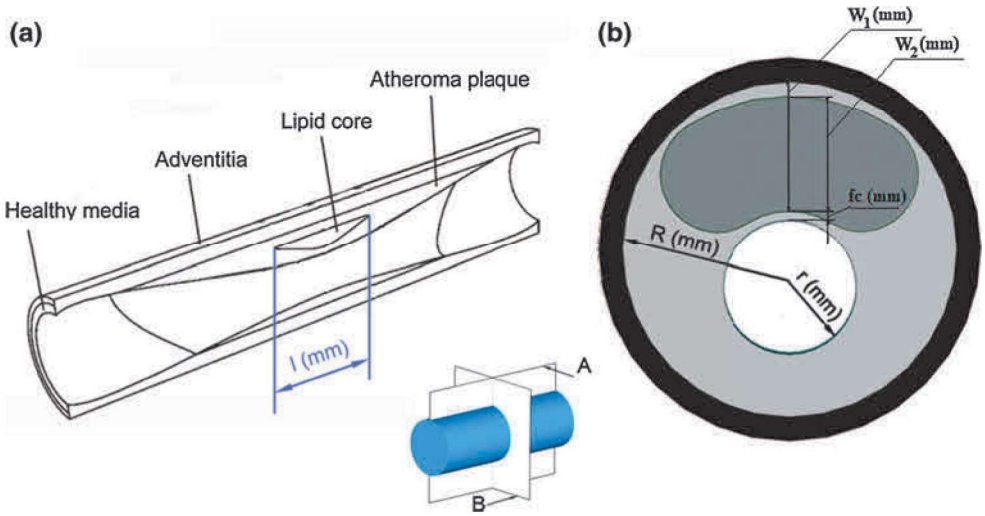

Fig. 1 **a** Idealized geometry of an atherosclerotic arterial model. Transversal section. **b** Geometrical parameters shown on the cross central section of the atherosclerotic vessel

2.2 Material model and boundary conditions

All tissues were modelled as nonlinear, hyperelastic and incompressible materials (Carew et al. 1968; Holzapfel et al. 2005). The lipid core and the atherosclerotic plaque were modelled as isotropic materials, while healthy wall was considered as an anisotropic material with two families of fibres, oriented at $\pm 61.8°$ and $\pm 28.35°$ with respect to the circumferential direction in the adventitia and the media layers, respectively. Both families of fibres were assumed to have the same mechanical properties (Holzapfel et al. 2005). The behaviour of the tissue was modelled by using the Gasser, Ogden and Holzapfel (GOH) strain energy function (SEF) (Gasser et al. 2006)

$$\begin{aligned}\Psi &= \mu[I_1 - 3] \\ &+ \frac{k_1}{2k_2}\left[\left[\exp\left(k_2\left[\kappa[I_1 - 3] + [1 - 3\kappa][I_4 - 1]\right]^2\right) - 1\right]\right. \\ &+ \left.\left[\exp\left(k_2\left[\kappa[I_1 - 3] + [1 - 3\kappa][I_6 - 1]\right]^2\right) - 1\right]\right],\end{aligned} \tag{1}$$

where $\mu > 0$ and $k_1 > 0$ are stress-like parameters and $k_2 > 0$ and $0 \leq \kappa \leq \frac{1}{3}$ are dimensionless parameters (when $\kappa = 0$ the fibres are perfectly aligned (no dispersion), and when $\kappa = \frac{1}{3}$ the fibres are randomly distributed and the material becomes isotropic), I_1 is the first invariant of $\mathbf{C} = \mathbf{F}^T\mathbf{F}$ with $\mathbf{F}$ the deformation gradient tensor, $I_4 = \mathbf{m}_0 \cdot \mathbf{C}\mathbf{m}_0$ and $I_6 = \mathbf{n}_0 \cdot \mathbf{C}\mathbf{n}_0$ are invariants which depend on the direction of the family of fibres at a material point $\mathbf{X}$ that is defined by the unit vectors field $\mathbf{m}_0$ and $\mathbf{n}_0$ (Spencer 1971).

To obtain the material parameters for the constitutive law of the tissue, experimental data presented in previous works [the adventitia and the media properties from Holzapfel et al. (2005) and the plaque and the lipid core properties from Versluis et al. (2006)] were fitted using the Levenberg–Marquardt minimization algorithm (Marquardt 1963). Table 2 shows the results of the parameter identification for each tissue.

The normalized mean square root error (ε) which is defined as

$$\varepsilon = \frac{\sqrt{\frac{\chi^2}{n-q}}}{\mu}, \tag{2}$$

was used to check the goodness of the fit. Where q is the number of parameters of the (SEF), n is the number of data points, $n - q$ is the number of degrees of freedom, and μ is the mean stress.

Regarding the boundary conditions, the longitudinal displacements were constrained at the end of the vessel, whereas the radial displacement was allowed. Symmetry conditions were imposed in the corresponding symmetry planes. In order to introduce the circumferential residual stress, a cut with an opening angle of 23.5° was performed in the opposite side of plaque location according to the experimental data of severe atherosclerosis obtained by Jaroslav et al. (1999). The opened model was closed such that we finally obtain the configuration shown in Fig. 1. To introduce the longitudinal residual stress, the model was stretched a 4.4 % of the vessel length in the longitudinal direction, representing in vivo conditions (Holzapfel et al. 2005). Then, a constant internal pressure of 140 mmHg (18.7 kPa) was imposed in the inner surface of the lumen, simulating the blood flow pressure (Ohayon et al. 2008).

Maximal principal stresses (MPS) were considered as the mechanical factor for the purposes of comparison in this study.

Table 2 Material parameters used in the finite element analysis for the adventitia, the healthy media, the atheroma plaque and the lipid core

	μ (kPa)	k_1 (kPa)	k_2 (−)	κ (−)	ε (−)
Adventitia	8.44	547.67	568.01	0.26	0.041
Healthy media	1.4	206.16	58.55	0.29	0.014
Atheroma plaque	9.58	17654.91	0.51	0.33	0.056
Lipid core	0.052	965.76	70	0.33	0.03

3 Results

It is important to remark that the maximum MPS was measured at the critical zones and always appeared in the circumferential direction. Some authors have shown that the maximum MPS sometimes appears at healthy areas, where the rupture is unlikely (Tang et al. 2005, 2008, 2009). Healthy areas where rupture is not probable, even if a local stress maximum occurred there, have been excluded from the analysis of the results.

3.1 Statistical analysis

To assess the influence of the geometrical parameters on the MPS, a statistical analysis was performed. The Lilliefors test (checking the normality of the distribution), the Student's t Tests and the analysis of variance (ANOVA) were used. The ANOVA test and the Student's t Test were performed at 1 and 5% significance level, respectively. Figure 2 shows the statistical analysis performed on the maximum MPS value in the critical region with respect to the distinct geometrical parameters for the three different studied cases (see Sect. 2.1). Each subfigure represents the results grouped for the different levels of each geometrical parameter, and the variation of this parameter becomes influential if the MPS is modified significantly as this parameter varies.

In the first row of Fig. 2, the median for each variation of the lipid core length increases slightly with the lipid core length for all the cases, especially in the axial and circumferential RS case. For the cases with axial RS and without RS, considering all the two-sample comparisons (paired t test), some significant differences are found, between the second group ($l = 2$ mm) and the groups marked with $*^{(2)}$ and between the fifth group ($l = 8$ mm) and the groups marked with $*^{(5)}$ ($p < 0.01$, see Fig. 2). However, when the circumferential and the axial RS are considered, the lipid core length becomes more influential since the means are always significantly different for all the two-sample lipid core length comparisons considered ($p < 10^{-5}$).

The stenosis ratio statistical analysis is shown in the second row of the Fig. 2. The medians and the dispersion are similar, and very few significant differences between the means of the groups for the three cases considered are found.

The statistical analysis of the fibrous cap thickness is shown in the third row of Fig. 2 and proves the influence of this parameter on the MPS for the three analysed cases (Sect. 2.1). A noteworthy remark is that the median, and the dispersion of each variation of the fibrous cap thickness decreases dramatically as the fibrous cap thickness increases. Considering all the two-sample fibrous cap thickness combinations, the means are always significantly different ($p < 10^{-5}$), reflecting the huge influence of this parameter on the MPS values, even if the RS are not considered.

Finally, the lipid core width statistical analyses shown in the fourth row of Fig. 2, shows that both medians and dispersions increase with the lipid core width. In a similar way than in the case of the fibrous cap thickness, for all the two-sample lipid core width considered comparisons, the means are always significantly different ($p < 10^{-5}$) for the three studied cases, showing again a high dependence on this parameter.

The general trend is that the maximum MPS increases if axial RS are considered, whereas the MPS decreases and the dispersion is reduced if circumferential and axial RS are included.

3.2 Vulnerability study

Regarding the vulnerability of the plaque, different threshold stress values have been proposed by different authors (Lendon et al. 1991; Cheng et al. 1993; Loree et al. 1994; Ohayon et al. 2005). In this study, a threshold value of 247 kPa has been used according to the set of experimental data obtained by Loree et al. (1994), assuming a normal distribution of the data. This threshold value indicates that the probability of having plaque rupture is 0.95 for the cases whose combination of parameters have a maximum MPS equal or higher than 247 kPa, according to the data by Loree et al. (1994).

The maximum MPS for each combination of parameters is shown in Figs. 3 and 4. The two most influential parameters, the fibrous cap thickness and the lipid core width (fc and w), were chosen as the variable represented by the surfaces. In each subfigure, five surfaces are presented, one for each sr variation. The safety threshold plane at 247 kPa is presented. The results obtained for the three cases (with axial RS, with circumferential and axial RS and without them) have been compared in both Figs. 3 and 4.

For the save of clarity, the contour maps of the maximum MPS that are higher than the safety threshold plane (the intersections between each surface of Fig. 3 and the safety threshold of 247 kPa plane for a lipid core length given) are shown in Fig. 4. According to the literature, the fibrous cap thickness has been considered to be the most important risk factor for the plaque rupture, but it is not the only one.

Interestingly, the obtained contour maps change for the different studied cases. For the case without RS, similar contour maps are obtained for $l = 4$, $l = 6$ and $l = 8$ mm, showing that the MPS has a strong dependency on the lipid core width (vulnerability limit of $w > 60\%$). Despite the fact that the lines corresponding to each variation of sr intersect in some cases, the vulnerability area increases as the stenosis ratio decreases. In every case, the vulnerable threshold of the fibrous cap thickness is between 0.025 and 0.01 mm.

However, the obtained contour maps can be classified into two groups according to the value of the lipid core length if axial RS are included, showing the high dependency on that parameter of the MPS. The first group includes the small atheroma plaques ($l \leq 2$ mm), the lipid core width, and the stenosis ratio have an important influence on the MPS (atheroma plaque becomes vulnerable for $w > 50\%$). The second group includes the long ones ($l \geq 4$ mm), the influence of w is less important, being more vulnerable for high values of w. A linear trendline is observed, being the vulnerable fibrous cap thickness threshold around 0.05 mm for low w values and 0.075 mm for high w values. Again, despite the fact that the lines corresponding to each variation of sr intersect in some cases, the vulnerability area increases as the stenosis ratio decreases.

Finally, if circumferential and axial RS are included, the obtained contour maps can also be classified into two groups as a function of the lipid core length, showing a strong dependency on that parameter of the MPS: first group for the small atheroma plaques ($l \leq 2$ mm), where there is not vulnerable geometries, and second group for the long ones ($l \geq 4$ mm), where the influence of w is important (atheroma plaque become vulnerable for $w > 55\%$). In every case, the vulnerable fibrous cap thickness threshold is around 0.05 mm.

It can be seen that the axial residual stresses reduce the dependency between the MPS and the lipid core width except for the smallest lipid core length ($l = 1$ mm). Interestingly,

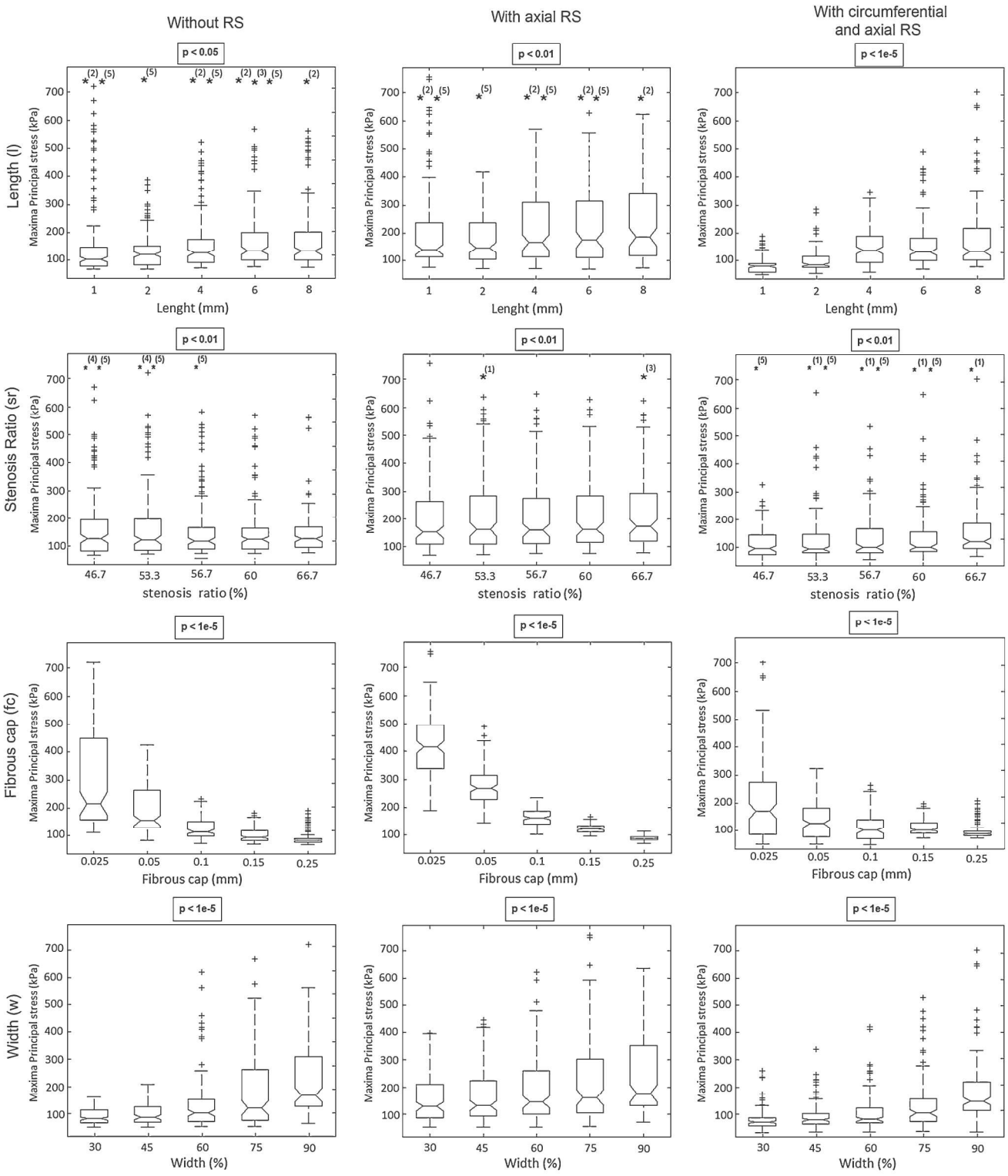

Fig. 2 Statistical analysis: Maximum MPS versus the variation of each parameter for the three different cases; without RS, with the axial RS included and with the circumferential and the axial RS included. The means of group n and the groups marked with $*^{(n)}$ are significantly different with the probability (p) indicated in the legend which is located in the top of each figure. Figures without any mark mean performing two-sample comparisons, the means are always significantly different. On each box, the central mark is the median, the edges of the box are the 25 and 75th percentiles, the whiskers extend to the most extreme data points not considered outliers, and outliers are plotted individually

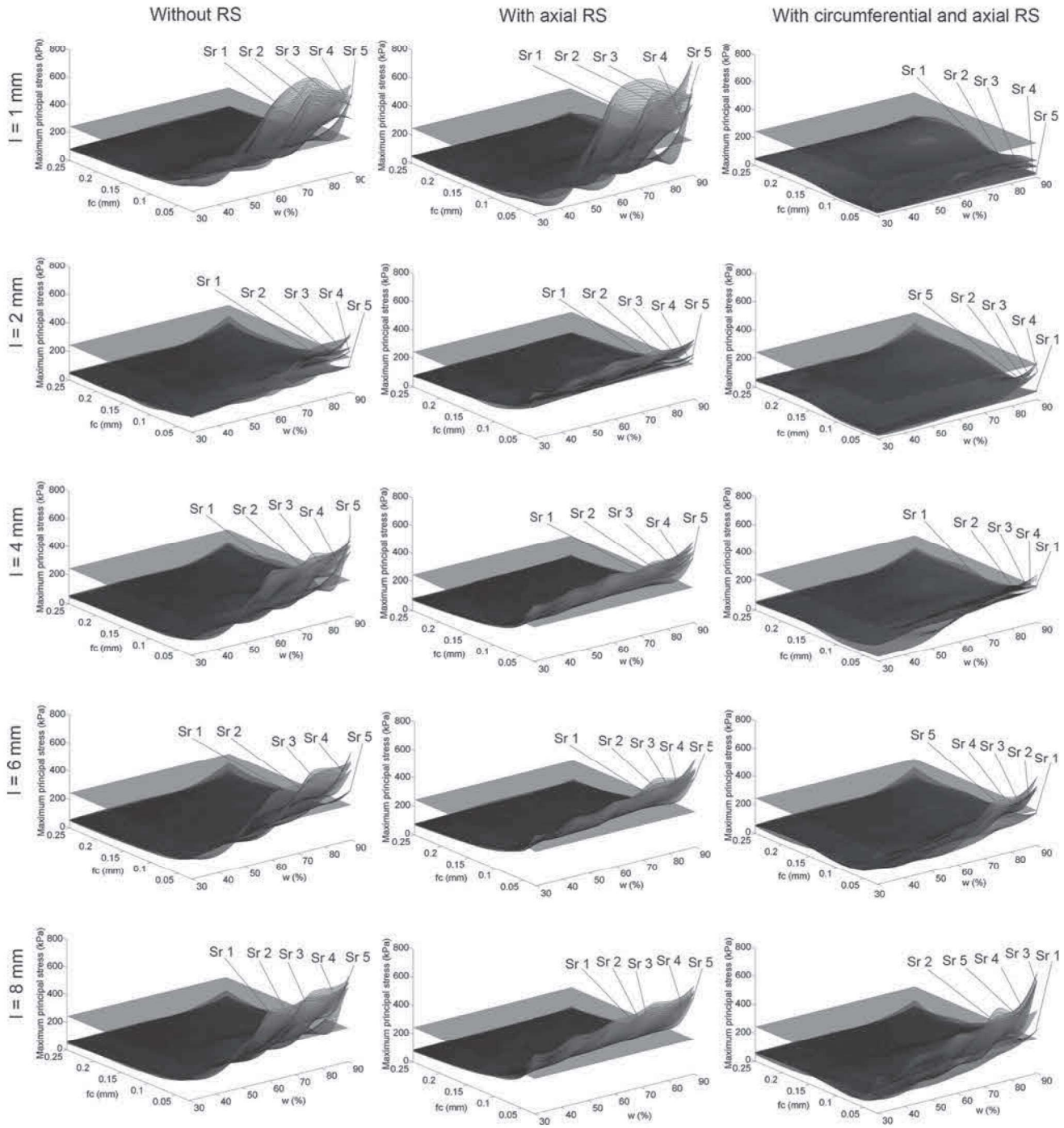

Fig. 3 Maximum MPS surfaces for a given lipid core length for the three cases studied; Without RS, with the axial RS included and with the circumferential and the axial RS included

the axial residual stresses dramatically increase the vulnerable area showing MPS values higher than 247 kPa for small values of the lipid core width. However, the circumferential and the axial residual stresses together produce again a strong dependency between the MPS and the lipid core width, and the vulnerable area highly decreases due to the effects of compression stress in the inner layer of the vessel fibrous cap zone, produced by the circumferential RS. This fact shows the relevance of considering the residual stresses in the vulnerability computational analysis of the plaque.

Figure 5 illustrates the difference between the results obtained in an idealized 3D model with the longitudinal RS

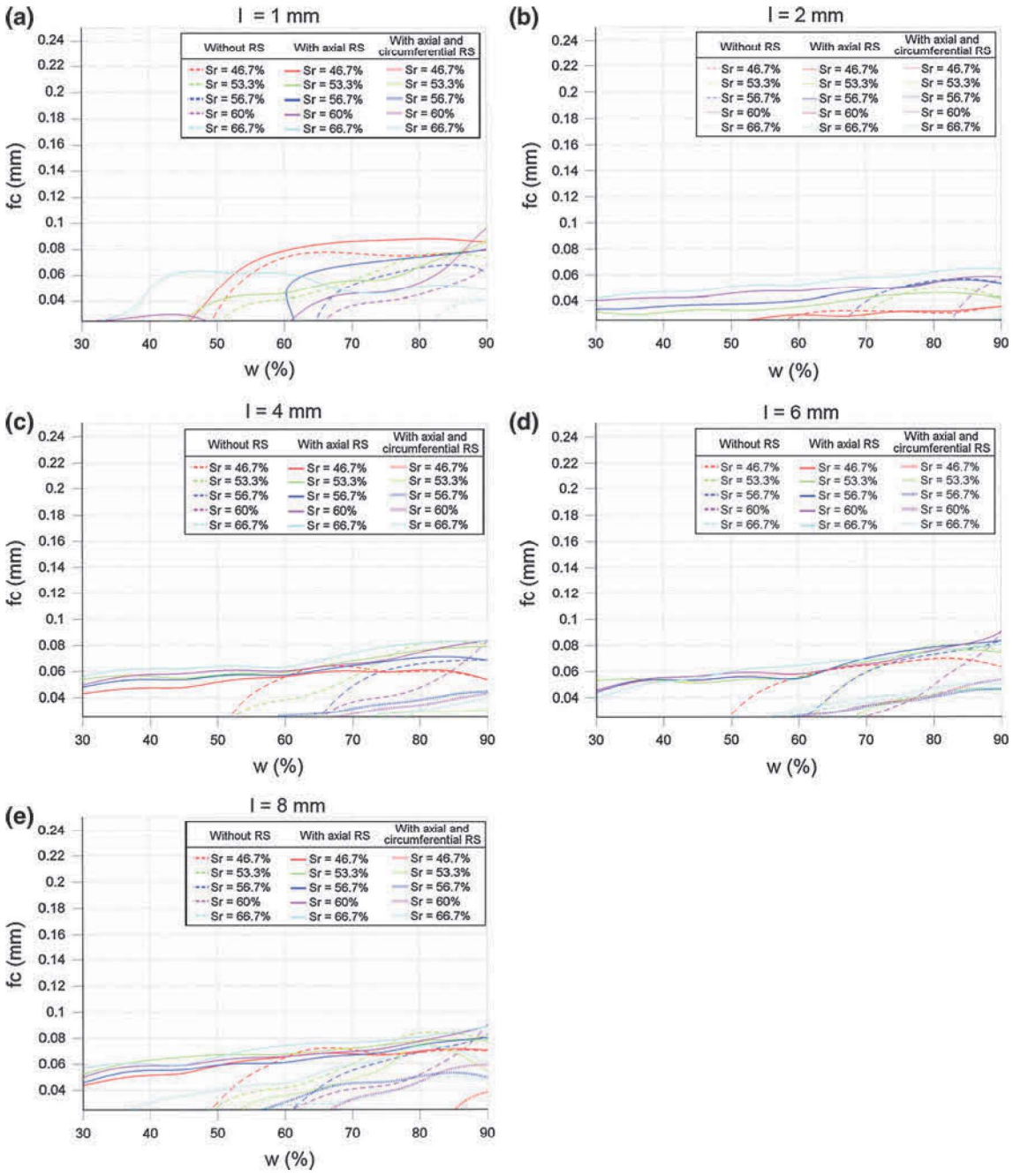

Fig. 4 Contours of the intersection between the safety threshold plane (247 kPa) and the maximum MPS surfaces for all *l* studied and for the results without RS, with the axial RS included and with the circumferential and the axial RS included

included (Fig. 5a), a 3D model with the circumferential and the longitudinal RS included (Fig. 5b) and the equivalent 3D model without residual stresses (Fig. 5c). The dimensions of the presented case are 4 mm long lipid core, 53.3% of stenosis ratio, 0.025 mm thick of fibrous cap, and 60% of lipid core width. The maximum MPS is located at the fibrous cap in every case; however, it value varies from 451.7 kPa in the model with the axial RS included, to 254.4 in the with circumferential and the axial RS included and to 385.7 kPa in the model without residual stress effects. The maximum MPS decreases with the incorporation of circumferential and axial RS, but increases when just the longitudinal RS are considered. However, although this trend is observed in a great number of cases, it could not be completely generalized. It also highly depends on the geometrical factors, as it is shown in Fig. 4.

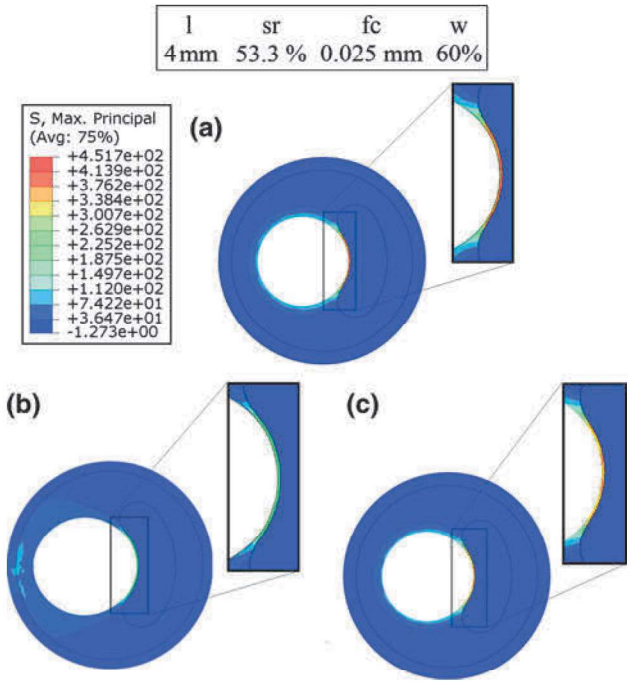

Fig. 5 Contour maps of MPS. Comparison between a model with the longitudinal RS included (**a**), a model with the longitudinal and the circumferential RS included (**b**) and without them (**c**)

3.3 Vulnerability factor

In order to quantify the vulnerability risk, a vulnerability factor (VF) was used. This factor is defined as

$$\mathrm{VF} = \frac{\text{Maximum MPS (kPa)}}{\text{Critical MPS (kPa)}}, \tag{3}$$

where the critical MPS value is assumed to be 247 kPa.

For the 625 cases in which circumferential and axial RS were included, the values of the VF for the main combinations of parameters which produce a maximum MPS higher than 247 kPa (Fig. 4) are shown in Tables 3, 4 and 5. In each table, the lipid core width is considered constant, the fibrous cap thicknesses are 0.025 mm (left sides of the tables) and 0.05 mm (right sides of the tables) and the lipid core length and the lumen radius vary.

Generally, the VF values in Tables 4 and 5 are higher than in Table 3 for the same values of l and sr, showing the dependency on w of MPS. It can be observed that the VFs increase with w. Most of the VFs are lower than 1 for the small values of l ($l \leq 2$ mm) and higher than 1 for the long ones ($l \geq 4$ mm), which show the dependence on l of MPS. A positive relation was observed between the increase in fc and the VF since the values of the VFs are significantly higher in the left sides of the tables ($fc = 0.025$ mm) than in the right sides ($fc = 0.05$ mm). The highest vulnerability factor is 2.98 ($l = 8$ mm, $sr = 66.6\%$, $fc = 0.025$ mm and $w = 90\%$), exceeding the safety threshold value of 247 kPa by a factor of three, Table 5.

4 Discussion

Quantifying the mechanical stress in the wall of an atherosclerotic vessel and, more specifically, in the fibrous cap, is a vital step in predicting the risk of plaque rupture based on biomechanical features, especially in 3D geometries (Creane et al. 2010). For this reason, the mechanical behaviour of a 3D parametric atheroma plaque in a coronary vessel with atherosclerosis disease has been studied in this work by varying the four most influential geometrical parameters, that is, l, sr, fc and w, and including RS effects. Static finite element analyses were performed in order to study a group of idealized plaque morphologies and to try to predict the vulnerable plaque rupture.

Historically, fibrous cap thickness has been considered the most important and almost the exclusive factor determining plaque vulnerability (Arroyo and Lee 1999; Briley-Saebo et al. 2007). To date, very few 3D computational studies have been carried out specifically to investigate the effect of the lipid core size on plaque stress distribution. Loree et al. (1994) and Tang et al. (2004) used a finite element model to study the influence of the lipid core width on plaque stress distribution in a small number of distinct models ($n = 6$ and $n = 3$, respectively). Imoto et al. (2005) came to the conclusion that the size of the lipid core had no influence on the peak circumferential stress, but as their models are particularized

Table 3 Vulnerability factors for $fc = 0.025, 0.05$ mm and $w = 60\%$

sr(%)/l(mm)	$fc = 0.025$ mm					$fc = 0.05$ mm				
	1	2	4	6	8	1	2	4	6	8
46.6	0.08	0.16	0.73	0.44	0.51	0.09	0.10	0.52	0.41	0.47
56.3	0.66	0.20	0.75	0.52	1.66	0.09	0.20	0.25	0.39	0.41
56.6	0.11	0.27	1.02	1.02	1.12	0.11	0.19	0.72	0.59	0.68
60	0.14	0.19	0.98	1.00	0.79	0.10	0.20	0.68	0.41	0.44
66.6	0.28	0.51	0.80	1.10	1.70	0.23	0.38	0.63	0.75	0.89

Table 4 Vulnerability factors for $fc = 0.025, 0.05$ mm and $w = 75\%$

sr(%)/l(mm)	$fc = 0.025$ mm					$fc = 0.05$ mm				
	1	2	4	6	8	1	2	4	6	8
46.6	0.08	0.18	0.86	0.71	0.79	0.08	0.11	0.61	0.52	0.63
56.3	0.59	0.44	1.04	1.52	1.82	0.35	0.39	0.67	0.65	1.09
56.6	0.11	0.32	1.16	1.31	2.14	0.10	0.25	0.81	0.72	0.85
60	0.55	0.22	1.10	1.64	1.70	0.11	0.23	0.77	0.52	0.59
66.6	0.32	0.59	1.05	1.34	1.94	0.25	0.47	0.71	0.88	1.16

Table 5 Vulnerability factors for $fc = 0.025, 0.05$ mm and $w = 90\%$

sr(%)/l(mm)	$fc = 0.025$ mm					$fc = 0.05$ mm				
	1	2	4	6	8	1	2	4	6	8
46.6	0.08	0.23	1.00	0.93	1.25	0.08	0.14	0.67	0.71	0.85
56.3	0.48	0.79	1.05	1.69	2.67	0.45	0.36	0.82	0.89	1.12
56.6	0.13	0.76	1.33	1.70	1.80	0.10	0.30	0.93	0.91	0.98
60	0.30	1.02	1.25	1.95	2.64	0.36	0.45	0.92	1.07	1.19
66.6	0.33	1.08	1.21	1.61	2.98	0.27	0.47	0.86	1.00	1.25

to concentric plaques, their conclusions are not generalizable to eccentric coronary lesions. Finet et al. (2004) carried out a 2D parametric study which showed that a combination of measures including the arterial remodelling index, the cap thickness, and the necrotic core area or thickness is necessary for prediction. Ohayon et al. (2005) compared the *in vivo* performance of 2D and 3D finite element models and concluded that 2D analysis tends to overestimate the amplitude of the maximum MPS; however, residual stresses are not considered. The distribution of RS and its effects on the stress field in 3D parametric atherosclerotic coronary plaques have never been studied in detail. Owing to the difficulty of estimation stresses and strains in real geometries, the influence of residual stresses is usually ignored in structural analyses intended to predict plaque rupture location. Ohayon et al. (2007) assessed RS and its impact on the in vivo stress distribution in human vulnerable coronary plaques, studying six real pathological epicardial coronary artery samples.

Regarding the importance of RS, many authors have studied the role of circumferential RS, but mainly in non-stenotic arteries. Holzapfel et al. (2005) performed statistical analysis to test for significant correlations between age and axial in situ stretch, and there were significant negative correlations between both. This suggests that axial in situ stretches of the human LAD coronary artery decrease with age. Varnava et al. (2002) simulated the effects of tissue ageing on residual strain in the main right and left (ramus circumflexus) human coronary arteries, based on experimental data, and they found that experimental opening angle scatters considerably with age. The factors affecting the opening angle are age, sex, and the degree of atherosclerosis. Besides, their study showed the effect of including the circumferential RS in the final stress distribution. The vessel artery wall is under tension in the inner layers and under compressive stress in the outer layers, for positive opening angles. The difference between both layers increases as the opening angle increases. This fact tends to make the circumferential stress more uniform in the arterial wall under the constant internal pressure.

The findings in the present study show a high dependency on some purely 3D parameters and factors on the MPS distribution, such as the lipid core length and the axial RS, affecting the vulnerability risk of the plaques. Figures 4 and 5 clearly show the influence of residual stresses since the vulnerable unsafe areas change when residual stresses are considered. The predominant trend is that the incorporation of axial RS increases the maximum MPS. However, the incorporation of axial and circumferential RS reduces the maximum MPS. Therefore, 3D plaque models red could produce more accurate predictions, and plane strain plaque models could not be enough to calculate a sufficiently accurate MPS distribution. Plane strain models not only overestimate the maximum MPS, as it is shown in the literature by Ohayon et al. (2005), Krishna Kumar and Balakrishnan (2005), Ohayon et al. (2007), but they also miss RS effects and other features as fibre orientation, which cannot be consider in 2D models (Holzapfel et al. 2005).

The general trend observed in this study is that the maximum MPS increases with the lipid core length, the lumen radius and the lipid core width, and also when the fibrous cap thickness decreases. Figures 3, 4 and Tables 3, 4 and 5 show

Table 6 Summary of vulnerable limits of fc and w for each different l independently of the sr parameter

	With axial RS		With circumferential and axial RS		Without RS	
	fc (mm)	w (%)	fc (mm)	w (%)	fc (mm)	w (%)
$l = 1$	$fc \leq 0.088$	$w \geq 50$	No vulnerable zone		$fc \leq 0.077$	$w \geq 50$
$l = 2$	$fc \leq 0.085$	No limit	$fc \leq 0.025$	$w \geq 95$	$fc \leq 0.050$	$w \geq 58$
$l = 4$	$fc \leq 0.080$	No limit	$fc \leq 0.052$	$w \geq 62$	$fc \leq 0.079$	$w \geq 52$
$l = 6$	$fc \leq 0.081$	No limit	$fc \leq 0.055$	$w \geq 64$	$fc \leq 0.079$	$w \geq 50$
$l = 8$	$fc \leq 0.082$	No limit	$fc \leq 0.080$	$w \geq 38$	$fc \leq 0.080$	$w \geq 50$

that the most of the parameter combinations have MPS values lower than 247 kPa (VF $<$ 1); however, an important vulnerable plaque region, where the maximum MPS value is higher than the safety threshold (VF $\geq$ 1), was found. This region is generally formed by low fibrous cap thickness values. Moreover, this unsafe region changes from the analysis in which axial RS are considered to the analysis in which RS effects are neglected (Fig. 4) since when just axial RS are included (without internal pressure), the circumferential stresses are positive. Thus, if axial RS and internal pressure are imposed, the circumferential stresses are higher than without considering axial RS. To summarize, the vulnerable plaque region corresponds to a combination of the following parameters: $w \geq 50\%$, $fc \leq 0.088$ mm for any lumen radius and lipid core length. Table 6 shows the fc and w vulnerable limits for each l and for all values of the lumen.

The fibrous cap thickness and the lipid core width and length have been shown in this study to be critical geometric parameters to the overall plaque stability, whereas it has been shown that the lumen radius influence is lower, but non-negligible. The influence of these parameters on plaque rupture is shown in Fig. 2.

Similar results were previously obtained by other authors. Ohayon et al. (2008) obtained slight higher limits of these parameters, probably because they performed a 2D study. However, the global trends were similar. The remodelling index (a parameter equivalent to the stenosis ratio) and the lipid core width had a positive correlation with the maximum MPS, while the fibrous cap thickness had a negative correlation with the maximum MPS. Similar trends were found by Virmani et al. (2000) where they suggested that atherosclerotic lesions with a fibrous cap thickness of less than 65 μ are most likely to rupture. Several studies in the literature shown that plaques containing a highly thrombogenic lipid-rich core are more at risk of rupture if the size of the lipid core is large and is less consistent. Several investigators have reported on the relation of the amount of extracellular gruel and plaque fissuring (Gertz and Roberts 1990; Davies et al. 1993; Pasterkamp et al. 2000; Douglas et al. 2011). Davies et al. (1993) estimated that when at least 40% of the plaque consists of lipid, an atheroma is at risk of rupture.

Some limitations of this study should be mentioned. First, an idealized straight geometry has been used to perform the parametric analysis. Second, the material model was assumed to be isotropic and incompressible for the fibrous plaque and the lipid core and anisotropic and incompressible for the wall vessel. However, these assumptions have been widely accepted as allowable for the assessment of the biomechanical properties of atherosclerotic lesions (Cheng et al. 1993; Loree et al. 1992). Third, the material properties and residual stresses have been taken from experimental data in the literature (Jaroslav et al. 1999; Holzapfel et al. 2005; Versluis et al. 2006).To the best of the authors' knowledge, there are no data of axial RS for isolated plaques in the literature, so the axial RS used corresponds to a non-stenotic artery. The opening angle was assumed to be constant for all of the geometries though it is known that it depends on the plaque geometry. Fourth, viscoelastic effects were not considered (Armentano et al. 1995, 2006; Peña et al. 2010). Fifth, the analysis does not reproduce the pulsatile nature of physiological blood pressure. Also, the fluid-structure interaction effects resulting from such cyclic loading were not considered (Kock et al. 2008). It was assumed that there were no shear stresses, torques, time-varying forces or flow-related forces. Only static blood pressure was considered to be acting on the lesion in the models. Nevertheless, it has been documented that the effect of fluid shear stress is insignificant when compared to the effect of tensile wall stresses as a direct component in plaque fracture dynamics (Huang et al. 2001; Himburg et al. 2004), although it is considered essential in plaque formation and growth. The estimation of stresses induced by the static pressure load has been proved to be valid to identify stress concentrations in atherosclerotic lesions (Cheng et al. 1993) since the location of stress concentration does not significantly differ between models including static pressure and models with complex dynamic pressure profiles. Sixth, although similar studies in the literature include other parameters such as the lipid core angle or the remodelling index which is related to the lumen radius, the present study takes into account four of the most influential parameters (Versluis et al. 2006; Ohayon et al. 2008). Several preliminary tests were performed to exclude the lipid

core angle as an influential parameter, see Supplementary data. Seventh, calcifications were not considered in order to simplify the study (Bluestein et al. 2008). Different properties of the atheroma plaque were not taken into account in this parametric study. Properties of calcified, cellular and hypocellular plaques have been identified by other authors (Loree et al. 1994). Finally, the 3D parametric study only could be validated qualitatively. To the best of the author's knowledge, it is not possible to measure the stress concentration in real atheroma plaques and to correlate with the main geometrical risk factors in vivo conditions and later verify the plaque rupture. Actually, in the literature, the only way to extract stress information is by performing computational simulations reproducing geometry and in vivo conditions, and validating the model qualitatively, measuring the geometrical risk factors, but not measuring directly the stresses.

Despite these limitations, this parametric study can be considered as an additional step towards the development of a tool to assist clinicians in the identification of vulnerable atheroma plaques. The large-scale computational analysis aids the clinical staff to identify the critical morphological parameters that indicate plaque vulnerability and the likelihood of rupture.

Acknowledgments The authors gratefully acknowledge research support from the Spanish Ministry of Science and Technology through research project DPI 2010-20746-C03-01, and CIBER initiative. CIBER-BBN is an initiative funded by the VI National R&D&i Plan 2008-2011, Iniciativa Ingenio 2010, Consolider Program, CIBER Actions and financed by the Instituto de Salud Carlos III with assistance from the European Regional Development Fund. Finally, we also thank the Diputación General de Aragón (DGA) for the financial support to M. Cilla through grant B137/09.

References

Alastrué V et al (2007) Assessing the use of the "opening angle method" to enforce residual stresses in patient-specific arteries. Ann Biomed Eng 35:1821–1837

Armentano R et al (1995) Effects of hypertension on viscoelasticity of carotid and femoral arteries in humans. Hypertension 26:48–54

Armentano R et al (2006) An in vitro study of cryopreserved and fresh human arteries: a comparison with ePTFE prostheses and human arteries studied non-invasively in vivo. Cryobiology 52:17–26

Arroyo LH, Lee RT (1999) Mechanisms of plaque rupture: mechanical and biologic interactions. Cardiovasc Res 41:369–375

Auer M et al (2006) 3-D reconstruction of tissue components for atherosclerotic human arteries using ex vivo high-resolution MRI. Med Imaging 25:345–357

Bluestein D et al (2008) Influence of microcalcifications on vulnerable plaque mechanics using FSI modelling. J Biomech 41:1111–1118

Briley-Saebo KC et al (2007) Magnetic resonance imaging of vulnerable atherosclerotic plaques: current imaging strategies and molecular imaging probes. J Magn Reson Imaging 26:460–479

Carew TE et al (1968) Compressibility of the arterial wall. Circ Res 23:61–86

Cheng G et al (1993) Distribution of circumferential stress in ruptured and stable atherosclerotic lesions. A structural analysis with histopathological correlation. Circulation 87:1179–1187

Chun Y et al (2010) Three-dimensional carotid plaque progression simulation using meshless generalized finite difference method based on multi-year MRI patient-tracking data. Comput Model Eng Sci 57:51–76

Creane A et al (2010) Finite element modelling of diseased carotid bifurcations generated from in vivo computerised tomographic angiography. Comput Biol Med 40:419–429

Davies MJ (1996) Stability and instability: two faces of coronary atherosclerosis: the Paul Dudley White lecture 1995. Circulation 94:2013–2020

Davies MJ et al (1993) Risk of thrombosis in human atherosclerotic plaques: role of extracellular lipid, macrophage, and smooth muscle cell content. Br Heart J 69:377–381

Douglas AF et al (2011) Extracranial carotid plaque length and parent vessel diameter significantly affect baseline ipsilateral intracranial blood flow. Neurosurgery 69:114–121

Fayad ZA, Fuster V (2001) Clinical imaging of the high-risk or vulnerable atherosclerotic plaque. Circ Res 89:305–316

Finet G et al (2004) Biomechanical interaction between cap thickness, lipid core composition and blood pressure in vulnerable coronary plaque: impact on stability or instability. Coron Artery Dis 15:13–20

Fujii K et al (2005) Association of plaque characterization by intravascular ultrasound virtual histology and arterial remodeling. Am J Cardiol 96:1476–1483

Fuster V et al (2005) Atherothrombosis and high-risk plaque: part II: approaches by noninvasive computed tomographic/magnetic resonance imaging. J Am Coll Cardiol 46:1209–1218

Gao H, Long Q (2008) Effects of varied lipid core volume and fibrous cap thickness on stress distribution in carotid arterial plaques. J Biomech 41:3053–3059

Gasser TC et al (2006) Hyperelastic modelling of arterial layers with distributed collagen fibre orientations. J R Soc Interface 3:15–35

Gertz S, Roberts WC (1990) Hemodynamic shear force in rupture of coronary arterial atherosclerotic plaques. Am J Cardiol 66:1368–1372

Hanke CFG, Lenz H (2001) The discovery of the pathophysiological aspects of atherosclerosis—a review. Acta Chirurgica Belgica 101:162–169

Himburg HA et al (2004) Spatial comparison between wall shear stress measures and porcine arterial endothelial permeability. Am J Physiol Heart 286:H1916–H1922

Holzapfel GA et al (2005) Determination of the layer-specific mechanical properties of human coronary arteries with non-atherosclerotic intimal thickening, and related constitutive modelling. Am J Physiol Heart 289:H2048–H2058

Huang H et al (2001) The impact of calcification on the biomechanical stability of atherosclerotic plaques. Circulation 103:1051–1056

Imoto K et al (2005) Longitudinal structural determinants of atherosclerotic plaque vulnerability: a computational analysis of stress distribution using vessel models and three-dimensional intravascular ultrasound imaging. J Am Coll Cardiol 46:1507–1515

Jaroslav V et al (1999) Residual strain in human atherosclerotic coronary arteries and age related geometrical changes. Biomed Mater Eng 9:311–317

Jaroslav V et al (2002) Age related constitutive laws and stress distribution in human main coronary arteries with reference to residual strain. Biomed Mater Eng 12:121–134

Kips JG et al (2008) Identifying the vulnerable plaque: a review of invasive and non-invasive imaging modalities. Artery Res 2:21–34

Kock SA et al (2008) Mechanical stresses in carotid plaques using MRI-based fluid-structure interaction models. J Biomech 41:1651–1658

Krishna Kumar R, Balakrishnan KR (2005) Influence of lumen shape and vessel geometry on plaque stresses: possible role in the

increased vulnerability of a remodelled vessel and the shoulder of a plaque. Heart 91:1459–1465
Kyriacou S et al (1996) Finite element analysis of non-linear orthotropic hyperelastic membranes. Comput Mech 18:269–278
Lee R (2000) Atherosclerotic lesion mechanisc versus biology. Zeitschrift fur Kardiologie 89:80–84
Lee R et al (1993) Computational structural analysis based on intravascular ultrasound imaging before in vitro angioplasty: prediction of plaque fracture locations. J Am Coll Cardiol 21:777–782
Lendon CL et al (1991) Atherosclerotic plaque caps are locally weakened when macrophages density is increased. Atherosclerosis 87:87–90
Lloyd-Jones D et al (2009) Heart disease and stroke statistics–2009 update: a report from the American heart association statistics committee and stroke statistics subcommittee. Circulation 119:21–181
Loree H et al (1992) Effects of fibrous cap thickness on peak circumferential stress in model atherosclerotic vessels. Circ Res 71:850–858
Loree HM et al (1994) Static circumferential tangential modulus of human atherosclerotic tissue. J Biomech 27:195–204
Marquardt DW (1963) An algorithm for least-squares estimation of nonlinear parameters. SIAM J Appl Math 11:431–441
Moreno PR et al (2002) Intimomedial interface damage and adventitial inflammation is increased beneath disrupted atherosclerosis in the aorta: implications for plaque vulnerability. Circulation 105:2504–2511
Naghavi M et al (2003) From vulnerable plaque to vulnerable patient: a call for new definitions and risk assessment strategies: part I. Circulation 108:1664–1672
Ohayon J et al (2007) Influence of residual stress/strain on the biomechanical stability of vulnerable coronary plaques: potential impact for evaluating the risk of plaque rupture. Am J Physiol Heart 293:H1987–H1996
Ohayon J et al (2008) Necrotic core thickness and positive arterial remodeling index: emergent biomechanical factors for evaluating the risk of plaque rupture. Am J Physiol Heart 295:H717–H727
Ohayon J et al (2005) A three dimensional finite element analysis of stress distribution in a coronary atherosclerotic plaque: in-vivo prediction of plaque rupture location. Biomech Appl Comput Assist Surg 17:225–241
Ohayon J et al (2001) In-vivo prediction of human coronary plaque rupture location using intravascular and finite element method. Coron Artery Dis 12:655–663
Pasterkamp G et al (2000) Arterial remodeling in atherosclerosis, restenosis and after alteration of blood flow: potential mechanisms and clinical implications. Cardiovasc Res 45:843–852
Peña E et al (2010) A constitutive formulation of vascular tissue mechanics including viscoelasticity and softening behaviour. J Biomech 43:984–989
Peterson SJ, Okamoto RJ (2000) Effect of residual stress and heterogeneity on circumferential stress in the arterial wall. J Biomech Eng 122:454–456
Raghavan ML et al (2004) Three-dimensional finite element analysis of residual stress in arteries. Ann Biomed Eng 32:257–263
Salunke NV et al (2001) Compressive stress-relaxation of human atherosclerotic plaque. J Biomed Mater Res Part A 55:236–241
Smedby O (1998) Geometrical risk factors for atherosclerosis in the femoral artery: a longitudinal angiographic study. Ann Biomed Eng 26:391–397
Spencer AJM (1971) Theory of invariants. In: Continuum physics. Academic Press, New York, pp 239–253
Tang D et al (2009) Sites of rupture in human atherosclerotic carotid plaques are associated with high structural stresses: an in vivo MRI-based 3D fluid-structure interaction study. Stroke 40:3258–3263
Tang D et al (2004) Effect of a liqid pool on stress/strain distributions in stenotic arteries: 3D fluid-structure interactions (FSI) models. ASME J Biomech Eng 126:363–370
Tang D et al (2005) Local maximal stress hypothesis and computational plaque vulnerability index for atherosclerotic plaque assessment. Ann Biomed Eng 33:1789–1801
Tang T et al (2008) Correlation of carotid atheromatous plaque inflammation with biomechanical stress: utility of USPIO enhanced MR imaging and finite element analysis. Atherosclerosis 196:879–887
Thubrikar M (2007) Vascular mechanics and pathology. Spinger, Berlin
Vander Wal AC, Becker AE (1999) Atherosclerotic plaque rupture—pathologic basis of plaque stability and instability. Cardiovasc Res 41:334–344
VanEpps JS, Vorp DA (2007) Mechanopathobiology of atherogenesis: a review. J Surg Res 142:202–217
Varnava AM et al (2002) Relationship between coronary artery remodeling and plaque vulnerability. Circulation 105:939–943
Vengrenyuk Y et al (2006) A hypothesis for vulnerable plaque rupture due to stress-induced debonding around cellular microcalcifications in thin fibrous caps. Proc Natl Acad Sci 103:14678–14683
Versluis A et al (2006) Fatigue and plaque rupture in myocardial infarction. J Biomech 39:339–347
Virmani R et al (2006) Pathology of the vulnerable plaque. J Am Coll Cardiol 47:C13–18
Virmani R et al (2000) Lessons from sudden coronary death: a comprehensive morphological classification scheme for atherosclerotic lesions. Arterioscler Thromb Vasc Biol 20:1262–1275
Williamson SD et al (2003) On the sensitivity of wall stresses in diseased arteries to variable material properties. ASME J Biomech Eng 125:147–155